EUROPEAN ORGANIZATION FOR NUCLEAR RESEARCH

CERN – AB DEPARTMENT

Optics measurements for the LHC beam in the TT2-TT10 line and effect of the QKE58 suppression.

Elena Benedetto

Abstract

Dispersion and optics measurements in TT2-TT10 have been performed for the fast extracted LHC proton beam, to investigate the effect of the QKE58 doublet suppression in the PS (foreseen in 2007) in term of change in the optics parameters at the beginning of the transfer line and of injection mismatch in the SPS. In the note, the results of the November–2006 campaign are discussed and the tools used for the dispersion, Twiss parameters and beam profiles measurements are presented.

Geneva, Switzerland

22/10/07

1 Introduction

The main aim of the TT2-TT10 optics measurement campaign in November 2006 was to investigate the effect of the QKE58 suppression in the PS, in term of change in the optics parameters in the TT2-TT10 line, for the LHC-type beam. The QKE58, consisting of a doublet of quadrupoles, was used in the past for the extraction of electrons and anti-protons from the PS. In 2001 the hardware for the extraction of electrons and antiprotons has been dismantled but these magnets are still used to reduce the dispersion at the extraction septum SMH16 for all fast extracted beams. Recent measurements have shown that there is sufficient horizontal aperture in the septum to suppress the use of this doublet [1]. The plan is to remove it in the second half of 2007 run and recuperate the power converter for the Multi-Turn Extraction.

In order to determine the effect of the QKE58 suppression on the initial Twiss and dispersion parameters of the line, two sets of measurements have been done on 10th November 2006, with the MESPS beam (26 GeV proton LHC-type beam with low longitudinal emittance, $1 - 4$ bunches), first with QKE58 on and then with QKE58 off. Table 1 summarizes the parameters for the MESPS beam, used for measurements of dispersion, emittance and Twiss parameters.

In the following sections, the tools implemented and used for the data analysis will be described and then the measurement results will be presented.

beam	MESPS
Energy	26GeV
Intensity	$1\,10^{11}ppb$
ε_l	$0.25eV s$
$\varepsilon_x^* \cong \varepsilon_y^*$ (norm. rms)	$1\mu m\,rad$
# bunches	1 - 4
bunch rotation	no
momentum spread	$2.8\,10^{-4}$

Table 1: MESPS beam parameters used for the measurements of 10th November'06

2 Dispersion measurements

The dispersion measurements have been done by recording the transverse beam position at the pick-ups in TT2-TT10 and in SPS (first turn) via the *Passerelle*, a tool which provides access to PS and SPS equipments from Windows platform via Excel.

An Excel application developed by G. Arduini and D. Jacquet [2] has been used as a starting point to compute the dispersion at the beginning of the line.

For QKE58 on and off:

- the beam momentum is varied (by changing the reference frequency sent from SPS to PS)
- the transverse positions at the pick-ups is recorded
- for each momentum, the relative offset $(\Delta p/p)$ is computed from first turn measurements
- the dispersion D_i at each BPM location is obtained by a linear fit applied to the beam displacement as function of $(\Delta p/p)$
- a fit is applied to compute D_0 and D_0 at the beginning of TT2

The computation has been done by using the MAD-X optics model 2006 and the OTR monitors `F16.MTV201`, `BTV1018`, `BTV1024`, `BTV1025` and `BTV1026` have been added as additional constrains to the fit to get the dispersion at the beginning of the line.

2.1 Fit algorithm to get the dispersion at the beginning of TT2

2.1.1 Fitting with α

In the original version of the Excel application, the fitting function to obtain the horizontal dispersion at the beginning of the line is [2]:

$$D_i = C_i \bar{D}_0 + S_i \bar{D}'_0 + \alpha \tilde{D}_i \tag{1}$$

where C_i and S_i are the cos-like and sin-like function, $\tilde{D}_i$ is the dispersion for $D_0 = D'_0 = 0$ at the beginning of the line, α is a fit parameter introduced to take into account errors in the determination of the momentum offset, $\bar{D}_0 = D_0/\alpha$ and $\bar{D}'_0 = D'_0/\alpha$ are the measured initial conditions divided by the factor α. The function to be minimized with respect to $(\bar{D}_0, \bar{D}'_0, \alpha)$ is:

$$\chi^2 = \sum_{i=1}^{N} \left(\frac{D_i - (C_i \bar{D}_0 + S_i \bar{D}'_0 + \alpha \tilde{D}_i)}{\sigma_i} \right)^2 \tag{2}$$

leading to the system:

$$\begin{pmatrix} b & c & d \\ c & f & g \\ d & g & i \end{pmatrix} \begin{pmatrix} \bar{D}_0 \\ \bar{D}'_0 \\ \alpha \end{pmatrix} = \begin{pmatrix} a \\ e \\ h \end{pmatrix} \tag{3}$$

with:

$$a = \sum \frac{C_i D_{meas,i}}{\sigma_i^2} \qquad b = \sum \frac{C_i^2}{\sigma_i^2} \qquad c = \sum \frac{C_i S_i}{\sigma_i^2}$$

$$d = \sum \frac{C_i \tilde{D}_i}{\sigma_i^2} \qquad e = \sum \frac{S_i D_{meas,i}}{\sigma_i^2} \qquad f = \sum \frac{S_i^2}{\sigma_i^2}$$

$$g = \sum \frac{S_i \tilde{D}_i}{\sigma_i^2} \qquad h = \sum \frac{\tilde{D}_i D_{meas,i}}{\sigma_i^2} \qquad i = \sum \frac{\tilde{D}_i^2}{\sigma_i^2}$$

In this formulation, the measured dispersion is only on the right side of the linear system.

2.1.2 Fitting with β

The Excel application has been modified in order to take into account the possibility to have different calibration errors for the different kind of monitors.

As a first step, Eq.1 can be written as:

$$\beta D_{meas,i} = C_i D_0 + S_i D'_0 + \tilde{D}_i \tag{4}$$

obtained by introducing the parameter $\beta = 1/\alpha$. The function to be minimized with respect to the initial conditions (D_0, D'_0) and β is now:

$$\chi^2 = \sum_{i=1}^{N} \left(\frac{\beta D_{meas,i} - (C_i D_0 + S_i D'_0 + \tilde{D}_i)}{\sigma_i} \right)^2 \tag{5}$$

and the system to be solved is:

$$\begin{pmatrix} bb & cc & dd \\ cc & ff & gg \\ dd & gg & ii \end{pmatrix} \begin{pmatrix} D_0 \\ D'_0 \\ \beta \end{pmatrix} = \begin{pmatrix} aa \\ ee \\ hh \end{pmatrix} \tag{6}$$

With:

$$aa = -\sum \frac{C_i \tilde{D}_i}{\sigma_i^2} = -d \qquad\qquad bb = \sum \frac{C_i^2}{\sigma_i^2} = b$$

$$cc = \sum \frac{C_i S_i}{\sigma_i^2} = c \qquad\qquad dd = -\sum \frac{C_i D_{meas,i}}{\sigma_i^2} = -a$$

$$ee = -\sum \frac{S_i \tilde{D}_i}{\sigma_i^2} = -g \qquad\qquad ff = \sum \frac{S_i^2}{\sigma_i^2} = f$$

$$gg = -\sum \frac{S_i D_{meas,i}}{\sigma_i^2} = -e \qquad\qquad hh = \sum \frac{\tilde{D}_i D_{meas,i}}{\sigma_i^2} = h$$

$$ii = \sum \frac{D_{meas,i}^2}{\sigma_i^2}$$

In this case, the terms which contain the measured dispersion $D_{meas,i}$ are also in the left side of the system, thus errors in the measurements will change the matrix to be inverted as well.

2.1.3 Calibration factors β_k

Equation 4 is then extended to take into account different calibration factors for the different kind of monitors. At the i-th point on the line, it becomes:

$$\sum_{k=TT2,...,SPS}^{monitors} \beta_k \delta(k - m_i) D_{meas,i} = C_i D_0 + S_i D_0' + \tilde{D}_i \qquad (7)$$

where m_i is the type of monitor installed in the i-th measured point on the line.

The system to be solved is:

$$\mathbf{M} \begin{pmatrix} D_0 \\ D_0' \\ \beta_{TT2} \\ ... \\ \beta_{SPS} \end{pmatrix} = \begin{pmatrix} aa \\ ee \\ hh_{TT2} \\ ... \\ hh_{SPS} \end{pmatrix} \qquad (8)$$

with:

$$\mathbf{M} = \begin{pmatrix} bb & cc & dd_{TT2} & ... & dd_{SPS} \\ cc & ff & gg_{TT2} & ... & gg_{SPS} \\ dd_{TT2} & gg_{TT2} & ii_{TT2} & & 0 \\ ... & ... & & ... & \\ dd_{SPS} & gg_{SPS} & 0 & & ii_{SPS} \end{pmatrix} \qquad (9)$$

where the sums in dd_k, gg_k, ii_k, hh_k are extended over the measurements performed with the monitor $k = TT2, ..., SPS$ only:

$$dd_k = -\sum_{i=1}^{N} \frac{C_i D_{meas,i}}{\sigma_i^2} \delta(k - m_i)$$

$$gg_k = -\sum_{i=1}^{N} \frac{S_i D_{meas,i}}{\sigma_i^2} \delta(k - m_i)$$

$$hh_k = \sum_{i=1}^{N} \frac{\tilde{D}_i D_{meas,i}}{\sigma_i^2} \delta(k - m_i)$$

$$ii_k = \sum_{i=1}^{N} \frac{D_{meas,i}^2}{\sigma_i^2} \delta(k - m_i)$$

4

By solving the system, one gets the dispersion D_0 and its derivative D_0' at the beginning of TT2 and the calibration factors β_k for the different monitors. The statistical errors on these quantities are given by the diagonal term of the inverse of $\mathbf{M}$ (Eq. 9):

$$\delta D_0 = \sqrt{\mathbf{M}^{-1\,(11)}}$$
$$\delta D_0' = \sqrt{\mathbf{M}^{-1\,(22)}}$$
$$\delta \beta_k = \sqrt{\mathbf{M}^{-1\,(kk)}}$$

The fitted dispersion at each point in the line is:

$$D_{fit,i} = C_i D_0 + S_i D_0' + \tilde{D}_i \tag{10}$$

and has to be compared with the quantity $(\beta_k D_{meas,i})$.

The errors in the horizontal fitted dispersion is:

$$\delta D_{fit,i} = \sqrt{C_i^2 (\delta D_0)^2 + S_i^2 (\delta D_0')^2} \tag{11}$$

and the error in $(\beta_k D_{meas,i})$ is:

$$\delta(\beta_k D_{meas,i}) = \beta_k D_{meas,i} \sqrt{\left(\frac{\sigma_i^2}{D_{meas,i}}\right)^2 + \left(\frac{\delta \beta_k}{\beta_k}\right)^2} \tag{12}$$

In the vertical plane the measured dispersions are multiplied by the calibration factor β_k and the fit is computed as in [2], considering the error $\delta(\beta_k D_{meas,i})$ from Eq. 12. In doing this, it is assumed that the monitor calibration errors are the same in the horizontal and vertical planes.

3   Optics measurements

To compute the beam emittance and the Twiss parameters at the beginning of the TT2 line, the standard approach of the 3–monitor method (see e.g. [3, 4]) is extended to more than 3 monitor profiles, using a fitting procedure. We assume that:

- the transfer matrices between the monitors in the line are known as well as the transfer matrix from the beginning of TT2 line to the first profile monitor

- the dispersion at the monitor location and the momentum spread are known

- there is no coupling

As input we need the theoretical beta functions, alphas and phase advance at the monitor location: $\beta_{i,x(y)}$, $\alpha_{i,x(y)}$, $\mu_{i,x(y)}$, the dispersion at the monitor location: $D_{i,x(y)}$ and the r.m.s. momentum spread: (dp/p).

From the theoretical Twiss parameters we can compute the cos- and sine–like functions [5] from the reference point $s = s_0$ (e.g. the beginning of the line) to the i-th monitor at position $s = s_i$:

$$C_i \equiv C(s_i, s_0) = \sqrt{\frac{\beta_i}{\beta_0}} \left[\cos(\mu_i - \mu_0) + \alpha_0 \sin(\mu_i - \mu_0)\right] \tag{13}$$

$$S_i \equiv S(s_i, s_0) = \sqrt{\beta_i \beta_0} \sin(\mu_i - \mu_0) \tag{14}$$

The r.m.s. beam size measured at the i-th monitor is:

$$\sigma_{meas,i}^2 = \sigma_{\beta,i}^2 + D_i^2 (dp/p)^2 \tag{15}$$

where $\sigma_{\beta,i}$ is the r.m.s. betatron beam size and the second term is the contribution from the dispersion.

The betatron beam size can be written [5] in terms of the sin- and cos–like functions (Eq.13) and of the Twiss parameters at the beginning of the line:

$$\sigma_{\beta,i}^2 \equiv \varepsilon\beta_i = \varepsilon(C_i^2\beta_0 - 2C_iS_i\alpha_0 + S_i^2\gamma_0) \tag{16}$$

so by knowing σ_β at 3 or more locations, it is possible to obtain emittance and Twiss parameters at the reference point.

3.1 Standard 3–monitors method

In case of three monitors, the system [1] is:

$$\begin{pmatrix} C_1^2 & -2C_1S_1 & S_1^2 \\ C_2^2 & -2C_2S_2 & S_2^2 \\ C_3^2 & -2C_3S_3 & S_3^2 \end{pmatrix} \begin{pmatrix} \varepsilon\beta_0 \\ \varepsilon\alpha_0 \\ \varepsilon\gamma_0 \end{pmatrix} = \begin{pmatrix} \sigma_{\beta,1}^2 \\ \sigma_{\beta,2}^2 \\ \sigma_{\beta,3}^2 \end{pmatrix} \tag{18}$$

and it has to be solved for ($\varepsilon\beta_0$, $\varepsilon\alpha_0$, $\varepsilon\gamma_0$). Using the relation: $\beta\gamma - \alpha^2 = 1$, the emittance is obtained by:

$$\varepsilon = \sqrt{(\varepsilon\beta_0)\,(\varepsilon\gamma_0) - (\varepsilon\alpha_0)^2} \tag{19}$$

and, from that, one can get $\beta_0, \alpha_0, \gamma_0$ at the beginnning of TT2 line.

3.2 More than 3 monitors: fit procedure

In case of more than 3 monitors, again assuming D_i and (dp/p) known, we can apply a least-square fit procedure.

For every monitor (horizontal and vertical) it is:

$$\sigma_{\beta,i}^2 = \sigma_{meas,i}^2 - D_i^2 \left(\frac{dp}{p}\right)^2 \tag{20}$$

We want to minimize the function:

$$\chi^2 = \sum_{i=1}^{monitors} \left(\frac{\sigma_{\beta,i}^2 - \varepsilon(C_i^2\beta_0 - 2C_iS_i\alpha_0 + S_i^2\gamma_0)}{\Delta_i}\right)^2 \tag{21}$$

with respect to ($\varepsilon\beta_0$, $\varepsilon\alpha_0$, $\varepsilon\gamma_0$), where $\Delta_i \equiv \delta(\sigma_{\beta,i}^2)$ is the error associated to $\sigma_{\beta,i}^2$:

$$\Delta_i = 2\sqrt{\delta\sigma_{meas,i}^2\,\sigma_{meas,i}^2 + \delta D_i^2\,D_i^2\left(\frac{dp}{p}\right)^4 + D_i^4\,\delta\left(\frac{dp}{p}\right)^2\left(\frac{dp}{p}\right)^2} \tag{22}$$

---

[1]Note that the matrix refers to the parameters at the beginning of the line. In order to have the parameters at the first monitor, the matrix would be:

$$\begin{pmatrix} 1 & 0 & 0 \\ C_2^2 & -2C_2S_2 & S_2^2 \\ C_3^2 & -2C_3S_3 & S_3^2 \end{pmatrix} \begin{pmatrix} \varepsilon\beta_0 \\ \varepsilon\alpha_0 \\ \varepsilon\gamma_0 \end{pmatrix} = \begin{pmatrix} \sigma_{\beta,1}^2 \\ \sigma_{\beta,2}^2 \\ \sigma_{\beta,3}^2 \end{pmatrix} \tag{17}$$

After some mathematics, we get:

$$M \begin{pmatrix} \varepsilon\beta_0 \\ \varepsilon\alpha_0 \\ \varepsilon\gamma_0 \end{pmatrix} = \begin{pmatrix} a \\ e \\ h \end{pmatrix} \tag{23}$$

where:

$$M = \begin{pmatrix} b & c & d \\ c & f & g \\ d & g & i \end{pmatrix} \tag{24}$$

and:

$$
\begin{aligned}
b &= \sum \frac{1}{\Delta_i^2} C_i^4 & c &= -\sum \frac{1}{\Delta_i^2} 2C_i^3 S_i & d &= \sum \frac{1}{\Delta_i^2} C_i^2 S_i^2 \\
f &= \sum \frac{1}{\Delta_i^2} 4C_i^2 S_i^2 & g &= -\sum \frac{1}{\Delta_i^2} 2C_i S_i^3 & i &= \sum \frac{1}{\Delta_i^2} S_i^4 \\
a &= \sum \frac{1}{\Delta_i^2} C_i^2 \sigma_{\beta,i}^2 & e &= -\sum \frac{1}{\Delta_i^2} 2C_i S_i \sigma_{\beta,i}^2 & h &= \sum \frac{1}{\Delta_i^2} S_i^2 \sigma_{\beta,i}^2
\end{aligned}
\tag{25}
$$

The solution of the system, from which one can derive the beam parameters and the emittance (Eq.19), is given by:

$$\begin{pmatrix} \varepsilon\beta_0 \\ \varepsilon\alpha_0 \\ \varepsilon\gamma_0 \end{pmatrix} = M^{-1} \begin{pmatrix} a \\ e \\ h \end{pmatrix} \tag{26}$$

3.2.1 Error estimate

The statistical errors associated to the fit parameters ($\varepsilon\beta_0$, $\varepsilon\alpha_0$, $\varepsilon\gamma_0$) are:

$$\delta\,\varepsilon\beta_0 = \sqrt{\mathbf{M}^{-1\,(1,1)}} \tag{27}$$

$$\delta\,\varepsilon\alpha_0 = \sqrt{\mathbf{M}^{-1\,(2,2)}} \tag{28}$$

$$\delta\,\varepsilon\gamma_0 = \sqrt{\mathbf{M}^{-1\,(3,3)}} \tag{29}$$

Assuming that ε, β, α are not correlated, the error on the emittance can be deduced by applying the standard techniques of error propagation to Eq.19:

$$(\delta\varepsilon)^2 = \frac{(\delta\,\varepsilon\beta_0)^2\,(\varepsilon\gamma_0)^2 \,+\, (\delta\,\varepsilon\gamma_0)^2\,(\varepsilon\beta_0)^2 \,+\, 4(\delta\,\varepsilon\alpha_0)^2(\varepsilon\alpha_0)^2}{4\varepsilon^2} \tag{30}$$

And finally the errors on the measured Twiss parameters are:

$$(\delta\beta_0)^2 = \beta_0^2 \left(\frac{(\delta\,\varepsilon\beta_0)^2}{(\varepsilon\beta_0)^2} + \frac{(\delta\varepsilon)^2}{\varepsilon^2} \right) \tag{31}$$

$$(\delta\alpha_0)^2 = \alpha_0^2 \left(\frac{(\delta\,\varepsilon\alpha_0)^2}{(\varepsilon\alpha_0)^2} + \frac{(\delta\varepsilon)^2}{\varepsilon^2} \right) \tag{32}$$

3.3 Blow-up due to Coulomb scattering at the screens

In case the profile measurements are all taken at the same time, with all the OTRs inside the beam, the blow-up due to Coulomb scattering at the screens can be important and has to be taken into account in the emittance and Twiss parameters computation.

The Coulomb-scattering effect on the particle distribution is obtained by the convolution of the beam distribution function in the phase space with the beam-matter interaction probability function. Using

the covariance matrix formalism [6], it can be demonstrated [6, 7] that the covariance matrix of the convoluted distribution Σ'_x is given by the sum of the initial beam covariance matrix Σ_x and the covariance matrix of the scattering Σ_C:

$$\Sigma'_x = \Sigma_x + \Sigma_C \tag{33}$$

The same holds for the vertical plane.

The beam covariance matrix Σ_x before the monitor is:

$$\Sigma_x = \begin{pmatrix} \varepsilon\beta & -\varepsilon\alpha \\ -\varepsilon\alpha & \varepsilon\gamma \end{pmatrix} \tag{34}$$

and, for a thin screen, assuming no modification in the position at the exit of the foil but only a change in angle, the scattering covariance matrix is:

$$\Sigma_C = \begin{pmatrix} 0 & 0 \\ 0 & \langle\theta^2\rangle \end{pmatrix}, \tag{35}$$

where $\sqrt{\langle\theta^2\rangle}$ is the r.m.s. scattering angle [8]:

$$\sqrt{\langle\theta^2\rangle} = 2.557 \, \chi_{cc} \frac{\sqrt{t}}{E\beta_{rel}^2} \tag{36}$$

with

$$\chi_{cc}^2 \approx (0.39612 \times 10^{-3})^2 Z_s \frac{\rho}{W} \left[GeV^2 cm^{-1} \right] \tag{37}$$

The scattering angle depends on the energy of the incident protons E (in GeV), the screen thickness t (in cm), and the other properties of the scattering material through the parameter χ_{cc}^2, where ρ is the material density, $W = \sum_{i=1}^{N} n_i A_i$ is the molecular weight and Z_s is defined as:

$$Z_s = \sum_{i=1}^{N} n_i Z_i (Z_i + 1) \tag{38}$$

being n_i the number of moles of element i in a mole of material and Z_i the atomic number.

In Table 3.3 are summarized the material and scattering angles for the OTR screens in TT2-TT10, for protons at 26GeV.

3.3.1 Twiss parameter at the beginning of the line, scattering included

For a beam with covariance matrix $\Sigma_{x,0}$ at the beginning of the line (unknown):

$$\Sigma_{x,0} = \begin{pmatrix} \varepsilon\beta_0 & -\varepsilon\alpha_0 \\ -\varepsilon\alpha_0 & \varepsilon\gamma_0 \end{pmatrix}, \tag{39}$$

after transport in the line, the beam covariance matrix at $s = L$ is:

$$\Sigma_{x,L} = \mathbf{M}_L \, \Sigma_{x,0} \, \mathbf{M}_L^T \tag{40}$$

being $\mathbf{M}_L$ the transport matrix.

The transport matrices from the beginning of the line to the monitor i and between the monitor i and j are respectively:

$$\mathbf{M}_i = \begin{pmatrix} C_i & S_i \\ C'_i & S'_i \end{pmatrix} \quad, \quad \mathbf{M}_{ij} = \begin{pmatrix} C_{ij} & S_{ij} \\ C'_{ij} & S'_{ij} \end{pmatrix} \tag{41}$$

monitor	screen #	material	thickness	$\sqrt{\langle\theta^2\rangle}$
F16.MTV201 C	2	Carbon	$100\mu m$	$1.095\ 10^{-5}$
F16.MTV201 Ti-12	3	Titanium	$12\mu m$	$9.31\ 10^{-6}$
BTV1018 Al	1	Alumina	$1mm$	$3.57\ 10^{-5}$
BTV1018 Ti-12	2	Titanium	$12\mu m$	$9.31\ 10^{-6}$
BTV1018 M-25	3	Aluminized Mylar	$25\mu m$	$4.57\ 10^{-6}$
BTV1024 Al	1	Alumina	$1mm$	$3.57\ 10^{-5}$
BTV1024 Qu	2	Quartz	$1mm$	$5.27\ 10^{-5}$
BTV1024 M-25	3	Aluminized Mylar	$25\mu m$	$4.57\ 10^{-6}$
BTV1025 Al	1	Alumina	$1mm$	$3.57\ 10^{-5}$
BTV1025 Ti-12	2	Titanium	$12\mu m$	$9.31\ 10^{-6}$
BTV1025 M-25	3	Aluminized Mylar	$25\mu m$	$4.57\ 10^{-6}$
BTV1026 Al	1	Alumina	$1mm$	$3.57\ 10^{-5}$
BTV1026 Ti-8	2	Titanium	$8\mu m$	$7.6\ 10^{-6}$
BTV1026 M-25	3	Aluminized Mylar	$25\mu m$	$4.57\ 10^{-6}$

Table 2: OTR screens in TT2-TT10: materials and scattering angles

At the exit of the first monitor, the new beam matrix is:

$$\Sigma_{x,1} = \mathbf{M}_1\ \Sigma_{x,0}\ \mathbf{M}_1^T + \Sigma_{C,1} \tag{42}$$

where $\Sigma_{C,1}$ is the scattering covariance matrix at the first screen.
After the second monitor:

$$
\begin{aligned}
\Sigma_{x,2} &= \mathbf{M}_{12}\ \Sigma_{x,1}\ \mathbf{M}_{12}^T + \Sigma_{C,2} \\
&= \mathbf{M}_2\ \Sigma_{x,0}\ \mathbf{M}_2^T + \mathbf{M}_{12}\ \Sigma_{C,1}\ \mathbf{M}_{12}^T + \Sigma_{C,2}
\end{aligned} \tag{43}
$$

In general, at the exit of the i-th monitor, the beam matrix is:

$$\Sigma_{x,i} = \mathbf{M}_i\ \Sigma_{x,0}\ \mathbf{M}_i^T + \Sigma'_{C,i} \tag{44}$$

where $\Sigma'_{C,i}$ is the contribution from the scattering at the preceeding screens and it is known:

$$\Sigma'_{C,i} = \sum_{k=1}^{i-1} \left(\mathbf{M}_{ki}\ \Sigma_{C,k}\ \mathbf{M}_{ki}^T \right) + \Sigma_{C,i} \tag{45}$$

We are interested at the element (11) of $\Sigma_{x,i}$. From the measurements we get the first element of the beam covariance matrix:

$$\Sigma_{x,i}^{(11)} \equiv \sigma_{\beta_i}^2 = \sigma_{meas,i}^2 - D_i^2 (dp/p)^2 \tag{46}$$

The contribution from scattering is:

$$\Sigma'_{C,i}{}^{(11)} = \sum_{k=1}^{i-1} S_{ki}^2 \left\langle \theta^2 \right\rangle_k \tag{47}$$

and therefore:

$$
\begin{aligned}
\sigma_{\beta_i}^2 &= \left(\mathbf{M}_i\ \Sigma_{x,0}\ \mathbf{M}_i^T \right)^{(11)} + \Sigma'_{C,i}{}^{(11)} \\
&= C_i^2 (\varepsilon\beta_0) - 2 C_i S_i (\varepsilon\alpha_0) + S_i^2 (\varepsilon\gamma_0) + \Sigma'_{C,i}{}^{(11)}
\end{aligned} \tag{48}\tag{49}
$$

9

Again, by measuring σ_{β_i} at 3 monitor locations, it is possible to get $(\varepsilon\beta_0 \,,\; \varepsilon\alpha_0 \,,\; \varepsilon\gamma_0)$ at the reference point by solving the system:

$$\begin{pmatrix} C_1^2 & -2C_1S_1 & S_1^2 \\ C_2^2 & -2C_2S_2 & S_2^2 \\ C_3^2 & -2C_3S_3 & S_3^2 \end{pmatrix} \begin{pmatrix} \varepsilon\beta_0 \\ \varepsilon\alpha_0 \\ \varepsilon\gamma_0 \end{pmatrix} = \begin{pmatrix} \sigma_{\beta_i}^2 - {\Sigma'_{C,1}}^{(11)} \\ \sigma_{\beta_i}^2 - {\Sigma'_{C,2}}^{(11)} \\ \sigma_{\beta_i}^2 - {\Sigma'_{C,3}}^{(11)} \end{pmatrix} \tag{50}$$

where:

$$\begin{aligned} {\Sigma'_{C,1}}^{(11)} &= 0 \\ {\Sigma'_{C,2}}^{(11)} &= S_{12}^2 \left\langle \theta^2 \right\rangle_1 \\ {\Sigma'_{C,3}}^{(11)} &= S_{13}^2 \left\langle \theta^2 \right\rangle_1 + S_{23}^2 \left\langle \theta^2 \right\rangle_2 \end{aligned} \tag{51}$$

With respect to Eq.17, a new (known) term has appeared in the right side of the system, namely the quantity ${\Sigma'_{C,i}}^{(11)}$ has to be subtracted to the $\sigma_{\beta_i}^2$.

3.3.2 Extension to more than 3 monitors

The extension to more than 3 screens is straightforward, since, in the same way as for the 3–monitors method, if one replaces Eq. 20 by:

$$\sigma_{\beta,i}^2 = \sigma_{meas,i}^2 - D_i^2 \left(\frac{dp}{p} \right)^2 - {\Sigma'_{C,i}}^{(11)} \tag{52}$$

where ${\Sigma'_{C,i}}^{(11)}$ is the contribution from the Coulomb scattering at the preceeding screens computed in Eq. 47, the Equations 21 - 32 still apply.

4 Beam profiles at the BTV monitors

The 2D beam profiles have been recorded at the BTVs equipped with OTR screens in TT2-TT10 (`F16.MTV201, BTV1018, BTV1024, BTV1025, BTV1026`). The horizontal and vertical sizes are calculated by applying a bi-Gaussian fit, using a χ^2 minimization routine provided by Matlab. Before the fit is applied, a background image is removed, the beam is localized in the $254{\times}254$ pixel image and a tilted-elliptical window is selected for the fit. Moreover, since the screens are placed at $45°$ with respect to the beam and the CCD cameras have a finite focal length, the algorithm takes into account and correct for the induced image distortion.

4.1 Correction for CCD camera optics distortion

Since the screens are placed at $45°$ with respect to the beam and the CCD cameras have a finite focal length, the the acquired images are distorted, as shown in Fig. 1.

Before starting the measurements is therefore necessary to calibrate the monitors. Figure 1(left) is the image taken at `BTV1025`, without beam, using the Alumina screen, which has a grid of $1cm \times 1cm$ pitch size. It is possible to see that the number of pixels per cm N_p, which is the same in the horizontal and in the vertical planes, depends linearly on the vertical coordinate. In particular, once the center (x_0, y_0) of the image is found, it is:

$$N_p = n + m(y - y_0) \ [pixel/mm] \tag{53}$$

where n (the number of pixel per mm at the center of the image) and m (the linear coefficient) have to be determined. Note that the horizontal coordinate of the center x_0 has to correspond to the position of the grid line which is exactly vertical (indicated with an arrow in Fig. 1).
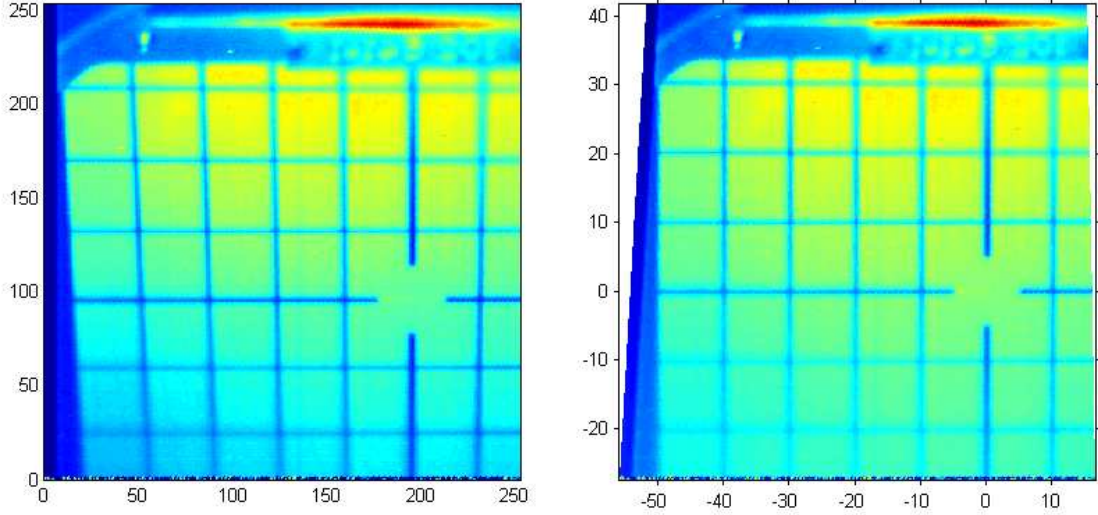
Figure 1: Left: Distorted image taken at BTV.1025, Alumina screen, before correction. Right: the same image after off-line correction.

The pixel size p_s has to be increased (decreased) according to the following equation:

$$p_s = \frac{1}{N_p} = \frac{1}{n + m(y - y_0)} \ [mm] \tag{54}$$

and the following calibration corrections have to be applied:

$$x^* = p_s(x - x_0) = \frac{x - x_0}{n + m(y - y_0)} \tag{55}$$

$$y^* = p_s(y - y_0) = \frac{y - y_0}{n + m(y - y_0)} \tag{56}$$

The pixel intensity as well depends on the vertical position of the pixel itself (if the pixel area is enlarged when applying the correction, its intensity has to be decreased proportionally, to keep the same density):

$$z^* = z \left(\frac{n + m(y - y_0)}{n} \right)^2 \tag{57}$$

For each monitor, the calibration and the center of the image (x_0, y_0) have to be determined during the calibration procedure.

4.2 Algorithm (momenta and fit)

A bi-Gaussian fit is applied to the images, by using the function:

$$f_G(x, y) = A\, e^{ -\frac{S_{22}(x - u_x)^2 + S_{11}(y - u_y)^2 - 2\, S_{12}(x - u_x)(y - u_y)}{2\, \det(S)} } + b \tag{58}$$

where the fitting parameter A is the maximum intensity, b is the offset, (u_x, u_y) are the centroid coordinates and S is the second order momenta matrix:

$$S = \begin{pmatrix} \langle XX \rangle & \langle XY \rangle \\ \langle XY \rangle & \langle YY \rangle \end{pmatrix} \tag{59}$$

11

and the beam sizes are:

$$\sigma_x = \sqrt{\langle XX \rangle} \tag{60}$$

$$\sigma_y = \sqrt{\langle YY \rangle} \tag{61}$$

The minimum of the χ^2:

$$\chi_{fit}^2 = \sum_i (z_i - f_G(x_i, y_i))^2 \tag{62}$$

is found with the *'fminsearch'* function from Matlab, which uses the simplex search method.

For every acquired image, after correcting for the CCD camera optics distortion, a background image obtained by an average over 8-10 shots without the beam can be subtracted, to remove systematic errors and offsets. The first part of the job is to localize the beam centroid and have a good first guess on the beam sizes and tilt, and then the bi-Gaussian fit is performed over the points inside a selected tilted-elliptical window.

To localize the beam centroid and have a good first guess on the beam horizontal and vertical sizes and correlation, which is needed for the Gaussian fit to converge, a quite elaborate algorithm has been used.

1. First of all a smoothing is applied by using a moving average over 4x4 points, to remove eventual spikes due to noise, and the points below a cut-off intensity ($z_{cut} = z_{MAX}/6$) are removed.

2. The first and second order momenta of the filtered distribution are computed.

3. The axis origin is shifted to the beam centroid estimated in Point 2

4. The filtered distribution is cut at 2σ of the tilted ellipse estimated from the second order momenta of Point 2 and the beam momenta are computed again

5. A first bi-Gaussian fit on the filtered distribution is performed using the momenta computed at Point 4 as a first guess

6. The values obtained at Point 5 are used to select a tilted-elliptical window (of 5σ) and as the initial guess to perform the fit on the raw data to get the actual beam sizes ad position.

4.3   1D-profiles at the SEM wires (and at the SEM grids) in TT2

In TT2 line, the SEM wires `MSG257, MSG267, MSG277` are used to record the horizontal and the vertical profile of 'small' beams such as the MESPS or the LHC beam, while for 'larger' beams such as AD, the 3 SEM grids `MSG258, MSG268, MSG278` are employed instead. The characteristics of these monitors are listed in Table 3.

monitor	# of channels	channel horiz. spacing	channel vert. spacing
MSG257	46	0.5 mm	0.5 mm
MSG267	46	0.35 mm	0.5 mm
MSG277	46	0.5 mm	0.5 mm
MSG258	16	2.5 mm	2.5 mm
MSG268	16	2.5 mm	2.5 mm
MSG278	16	2.5 mm	2.5 mm

Table 3: SEM grids and SEM wires in TT2

A 1D-Gaussian fit is applied to the profiles measured at these monitors. For the case of the SEM grids, since the size of the strips is not negligible with respect to the beam size and therefore the signal is an integral over a part of a Gaussian distribution, a correction factor [9] is applied to take into account the systematic error due to the strip size $d = 2mm$:

$$\mu_\sigma = \frac{\sigma_{meas} - \sigma_{beam}}{\sigma_{beam}} = \sqrt{1 + \frac{d}{12\sigma_{beam}}} - 1 \tag{63}$$
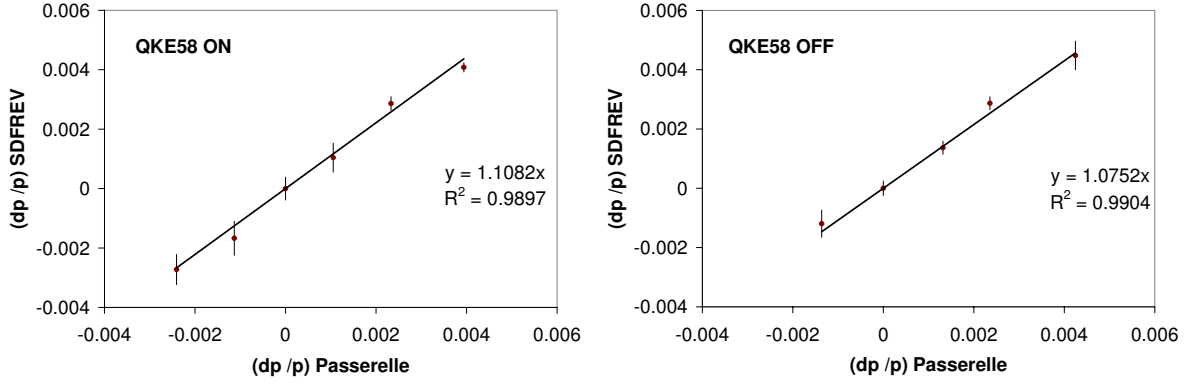
Figure 2: Momentum offset estimated from the reference frequency variation vs. the one computed within the application, for the cases with QKE58 on (left) and off (right). The standard error in the determination of the coefficient is 0.05 in both cases.

5 Measurements with MESPS beam and effect of QKE58 suppression

Having described the tools implemented and used in the data analysis, we now present the results of the measurement campaign in November '06

5.1 Dispersion measurements

For the two configurations with QKE58 powered and off, the dispersion at the beginning of TT2 line has been computed using the *Passerelle* and the tools described in Sec. 2, for an MESPS single bunch of nominal intensity ($1 \ 10^{11} ppb$), without bunch rotation. The beam momentum has been varied, by changing the reference frequency sent from the SPS to the PS, to cover a span of $\sim 5 \ 10^{-3}$ around its nominal value and 5 energy steps have been taken into account. The beam transverse displacement in both planes has ben recorded at the available monitors: 20 couplers in TT2-TT10, about 100 BPMs in the SPS, 3 SEM wires in TT2 and 5 OTRs in TT2-TT10. For each momentum step, an average over 6 measurements has been taken.

The momentum offset $(\Delta p/p)_m$ has been computed from the first turn horizontal BPM signals in the SPS and compared with the one $(\Delta p/p)_{ref}$, estimated from the reference frequency variation (SDFREV signal) via:

$$\left(\frac{\Delta p}{p}\right)_{ref} = \frac{1}{\eta_{PS}} \frac{\Delta f_{\text{SDFREV}}}{f_{\text{SDFREV}}} \ , \tag{64}$$

where η_{PS} is the PS slip factor at extraction ($26 GeV$):

$$\eta_{PS} = \frac{1}{\gamma^2} - \frac{1}{\gamma_{tr,PS}^2} \approx -0.025 \tag{65}$$

The $\gamma_{tr,PS}$ is computed using MADX and it is slightly different between the case with QKE58 ($\gamma_{tr,PS} = 6.0764$) and without QKE58 ($\gamma_{tr,PS} = 6.132$). Figure 2 shows that there is a difference of $\sim 10\%$ between the measured momentum offset and the reference one. The remaining discrepancy is due, on one side, to the uncertainties in the $\gamma_{tr,PS}$ and in the SDFREV signal and, on the other side, in the error bars in the $(\Delta p/p)_m$. In the following analysis, the momentum offset measured within the Excel application is used.

The dispersion at each monitor is obtained from a linear fit of the beam displacement as a function of momentum offset. Pick-ups which give a non realistic signal are taken out of the analysis. Finally, the dispersion at the 3 SEM wires and at the 5 OTRs in TT2-TT10 is computed outside the Excel application and the points are inserted in the fit algorithm to compute the dispersion at the beginning of the line.

	α–method	β_k–method	statistical error
$D_{0,x}$	2.914	2.892	0.014
$D'_{0,x}$	0.351	0.347	0.002
$\beta = 1/\alpha$	1.135		
β_{TT2} (β_{TT2}/β_{SPS})		1.62 (1.88)	0.039
β_{SEM} (β_{SEM}/β_{SPS})		0.951 (1.10)	0.029
β_{TT10} (β_{TT10}/β_{SPS})		1.159 (1.35)	0.012
β_{OTR} (β_{OTR}/β_{SPS})		0.917 (1.07)	0.030
β_{SPS} (β_{SPS}/β_{SPS})		0.859 (1.00)	0.013
$D_{0,x} SPS$	2.689	2.710	0.034
$D'_{0,x} SPS$	0.329	0.332	0.004
$\beta*_{SPS} = 1/\alpha*_{SPS}$	0.973	0.869	0.013
$D_{0,y}$	0.066	0.062	0.002
$D'_{0,y}$	-0.014	-0.015	0.001

Table 4: Dispersion results with QKE58 on, obtained by using either the α– or the β_k–method, with the statistical errors associated to the β_k–method. Either all the pick-ups in the line and SPS, either only the BPMs in the SPS are used for the fit ($D_{0,x} SPS$, $D'_{0,x} SPS$, $\beta*_{SPS}$). The vertical dispersion ($D_{0,y}$, $D'_{0,x}$) is computed by using all the available pick-ups.

	α–method	β_k–method	statistical error
$D_{0,x}$	3.939	3.913	0.013
$D'_{0,x}$	0.349	0.380	0.002
$\beta = 1/\alpha$	1.344		
β_{TT2} (β_{TT2}/β_{SPS})		1.725 (1.96)	0.016
β_{SEM} (β_{SEM}/β_{SPS})		0.939 (1.07)	0.052
β_{TT10} (β_{TT10}/β_{SPS})		1.065 (1.21)	0.007
β_{OTR} (β_{OTR}/β_{SPS})		0.786 (0.90)	0.035
β_{SPS} (β_{SPS}/β_{SPS})		0.877 (1.00)	0.011
$D_{0,x} SPS$	2.88	3.15	0.03
$D'_{0,x} SPS$	0.258	0.316	0.004
$\beta*_{SPS} = 1/\alpha*_{SPS}$	1.127	0.771	0.011
$D_{0,y}$	-0.072	0.084	0.002
$D'_{0,y}$	0.0074	-0.018	0.001

Table 5: Dispersion results with QKE58 off, obtained by using either the α– or the β_k–method. Either all the pick-ups in the line and SPS, either only the BPMs in the SPS are used for the fit.

To compute (D_0, D'_0) at the beginning of TT2, the method using the different β_k (Sec.2.1.3) has been used and has been compared with the original method [2] with α as a fitting parameter, showing very good agreement. Tables 4 and 5 present the results obtained for QKE58 on and off, by applying the α– or the β_k– methods. Only the statistical errors associated to the values computed with the β_k–method are reported, while the sensitivity of the pick-ups is not taken into account.

The suppression of QKE58 in the PS induces an increase of the horizontal dispersion at the beginning of TT2, from $\sim 2.9m$ to $\sim 3.9m$, while in the vertical plane the dispersion stays almost zero in the two cases, as expected.

By applying the β_k–method, the calibration factors for the different kind of monitors are also obtained. With respect to the SPS pick-ups calibration coefficient, there is a factor $\sim 90\%$ of difference

in the calibration of the first 10 couplers in TT2-TT10 (β_{TT2}) and a factor $\sim 30\%$ for the 10 couplers in the second chassis (β_{TT10}). Tables 4 and 5 show also the results obtained by fitting only on the point in the SPS. With respect to the fitting on the pick-ups in whole line, the dispersion at the beginning of TT2 looks smaller, and this is valid both using the $\alpha-$ or the $\beta-$method. This discrepancy, together with the large β_ks found for the TT2-TT10 pick-ups, has still to be understood and a calibration campaign is planned for 2007.

In the following, we will use the results obtained by using the β_k-method and the fit over all the TT2-TT10-SPS pick-ups.

Figures 3 and 5 show the horizontal dispersion at the pick-ups in the line and in the SPS 1st turn, respectively for the cases with QKE58 on and off. One can see an increase of the maximum value of the dispersion in the TT2-TT10 line from $\sim 4m$ to $\sim 9m$ if the QKE58 is switched off, together with a large mismatch in the machine. Figures 4 and 6 shows the theoretical horizontal dispersion in the ring and the measured points, respectively with the QKE58 on and off.

The blow-up after filamentation J in presence of dispersion mismatch, as defined in [10]:

$$J = 1 + \frac{\Delta D^2 + (\Delta D' \beta_0 + \Delta D \alpha_0)^2}{2\varepsilon\beta_0} \left(\frac{dp}{p}\right)^2 \tag{66}$$

in the horizontal plane it is equal to $J_{H,ON} = 1.07$ for QKE58 on, and $J_{H,OFF} = 2.08$ for QKE58 off, assuming a nominal LHC beam with normalized emittance $\varepsilon^* = 3 \times \mu m\,rad$ and $dp/p = 1.12 \times 10^{-3}$. ΔD (and $\Delta D'$) are the difference between the measured and the theoretical dispersion (and derivative) at a chosen point in the ring and β_0, α_0 are the corresponding Twiss parameters for the closed machine.

The vertical dispersion in the line and in the SPS 1st turn are plotted in Fig. 7 and 8. In the vertical plane there are almost no changes for the cases with QKE58 on and off, since the values of dispersion and its derivative at the beginning of the line stays almost zero. The computed blow-up factors are $J_{V,ON} = 1.002$ and $J_{V,OFF} = 1.005$ respectively.

5.2 Profile measurements and Twiss parameters computation at the beginning of TT2

The 1D horizontal and vertical beam profiles have been recorded at the SEM wires in TT2 (`MSG257`, `MSG267`, `MSG277`) and the 2D profiles at the BTVs, equipped with OTR screens, in TT2-TT10 (`F16.MTV201`, `BTV1018`, `BTV1024`, `BTV1025`, `BTV1026`). Many problems have been encountered to obtain good images at the BTVs in TT10, which have not been used for matching measurement since 2002. The CCD intensifiers have been replaced during summer 2006, because they had a non linear behavior (Fig. 9), but in 2006 the electronics was not yet part of the new control system, creating problems in the control of filters and especially of the acquisition timing. In 2007 the timing problems will be solved since also TT10 monitors will be included in the new standard.

For the profile measurements, an MESPS beam with 4 bunches of nominal intensity has been used, to increase the signal at the OTRs. The bunch rotation from the PS was switched off, in order to reduce the momentum spread and therefore the dispersion contribution to the beam size.

The horizontal and vertical beam sizes were computed at each monitor by applying a Gaussian fit to the beam profiles, as described in Sec. 4, and averaged over several measurements.

Tables 6 - 9 report the beam size measured at the screens, the dispersion which results from the measurements and fit presented in Sec. 5.1 and the informations about the scattering at the OTRs. The contribution of the dispersive part and of the scattering, both of them adding quadratically to the betatronic beam size $\sigma_{\beta,i}$ (Eq. 52), are also evaluated. In the horizontal plane it is necessary to minimize as much as possible the uncertainties on the determination of the momentum spread and of the dispersion itself, in order to have sufficient precision in the determination of the $\sigma_{\beta,i}$, since there are large values of dispersion at the screens. In the vertical plane, dispersion is always small except at `BTV1018`, where it contributes quadratically up to 44% of the beam size.
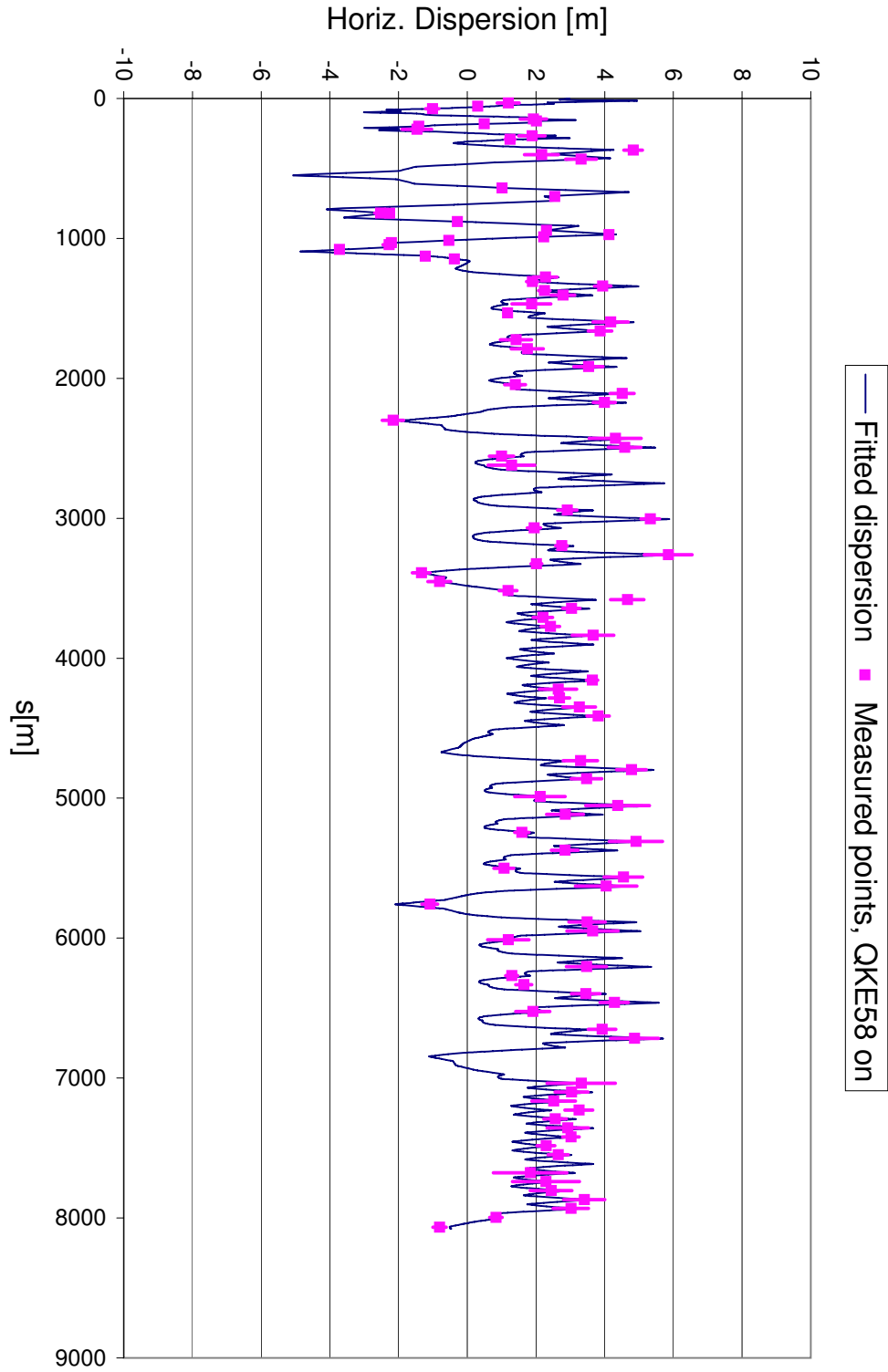
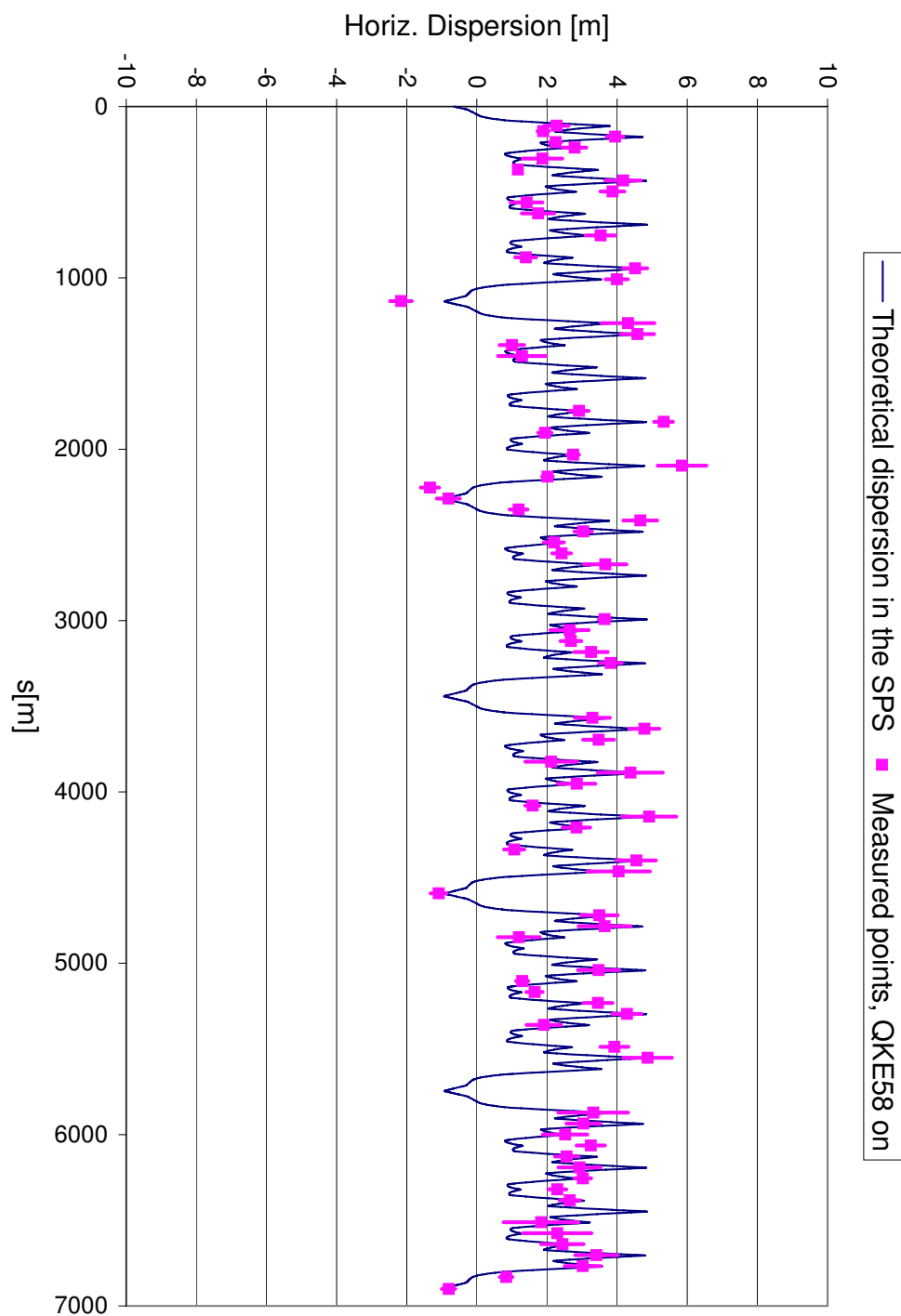Figure 3: Measured and fitted horizontal dispersion in TT2-TT10 and in the SPS 1st turn. QKE58 was on.

Figure 4: Measured horizontal dispersion at the SPS pick-ups (1st turn), compared with the theoretical one. QKE58 was on.
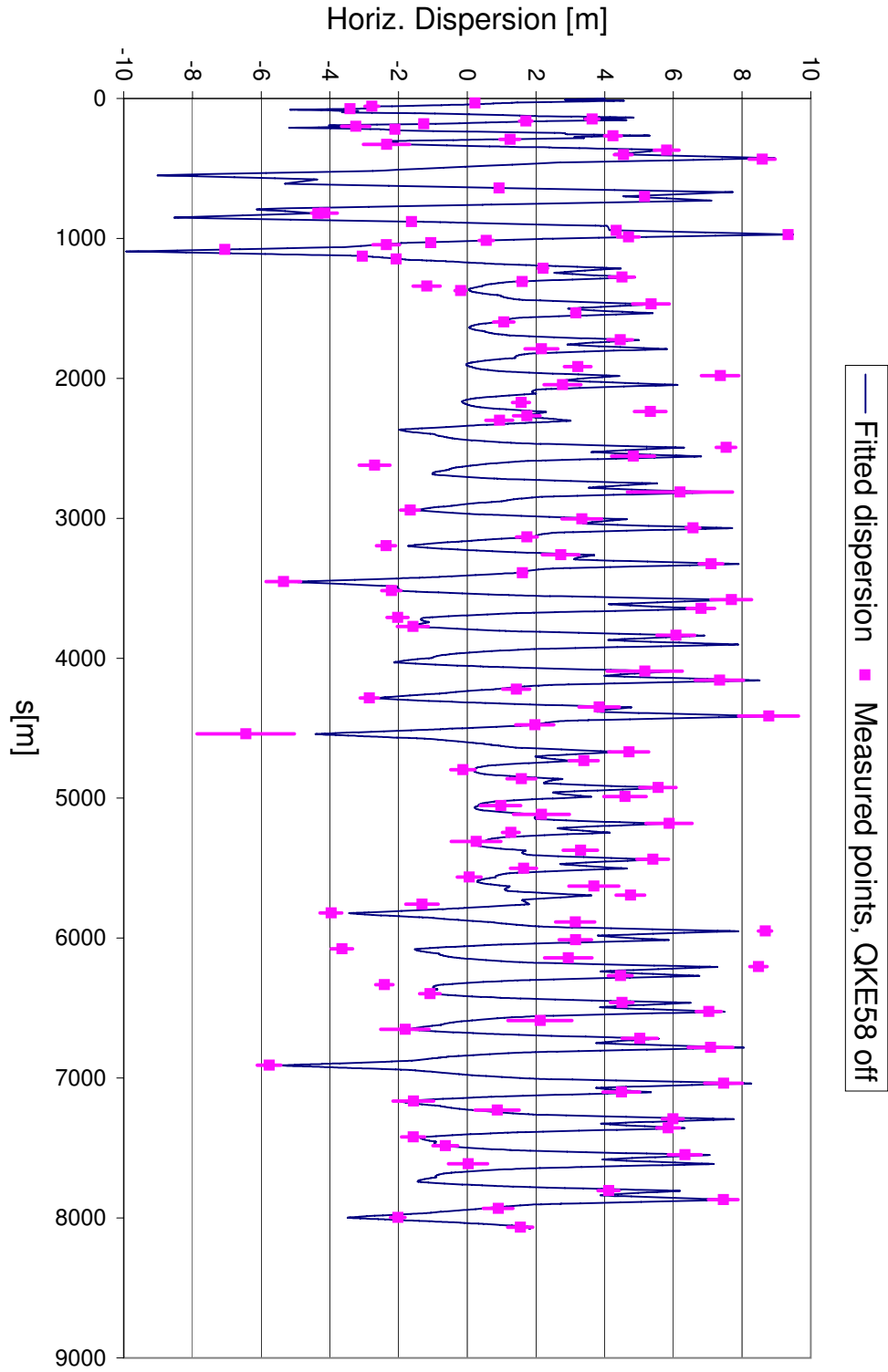
Figure 5: Measured and fitted horizontal dispersion in TT2-TT10 and in the SPS 1st turn. QKE58 was off.

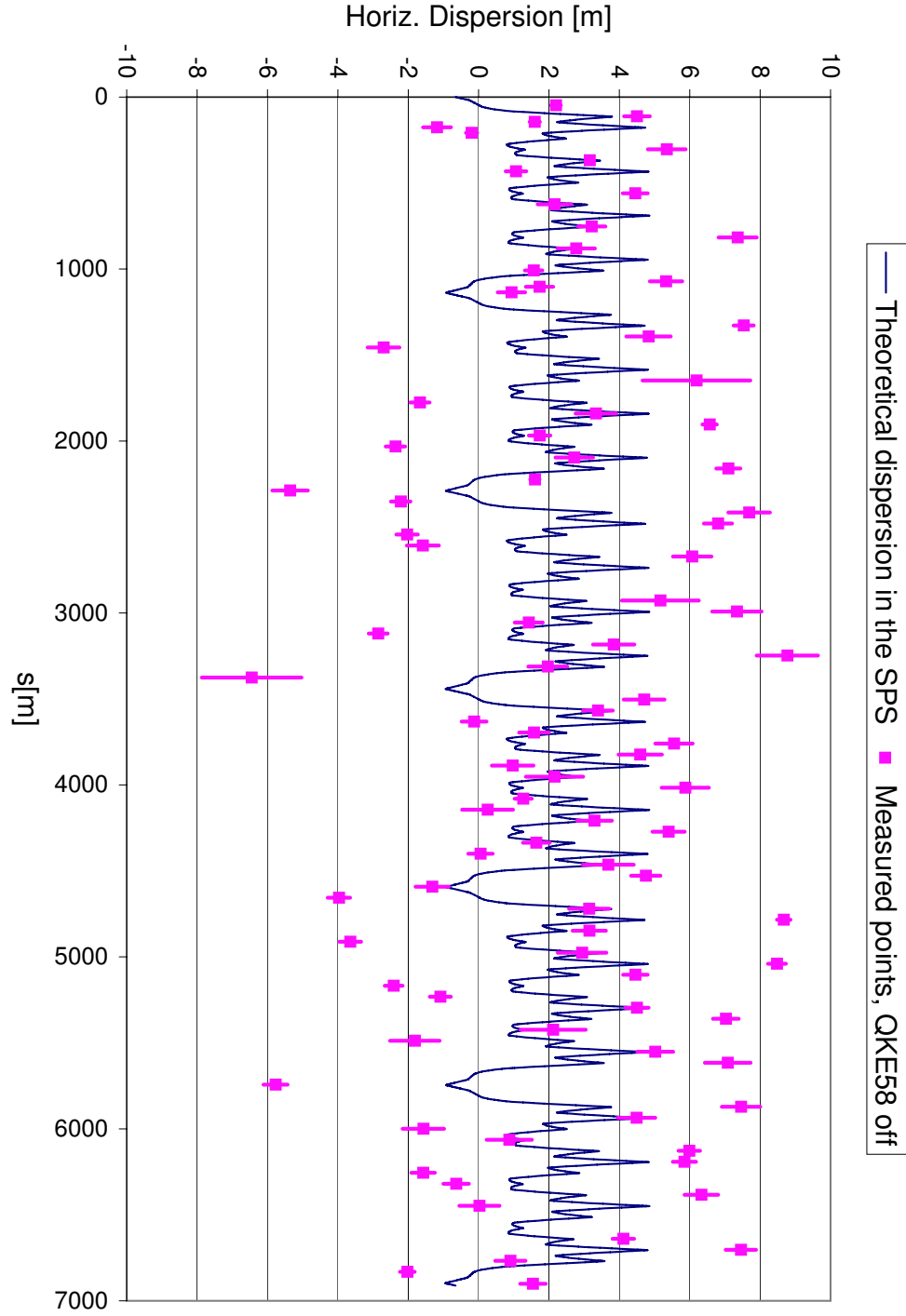Figure 6: Measured horizontal dispersion at the SPS pick-ups (1st turn), compared with the theoretical one. QKE58 was off.
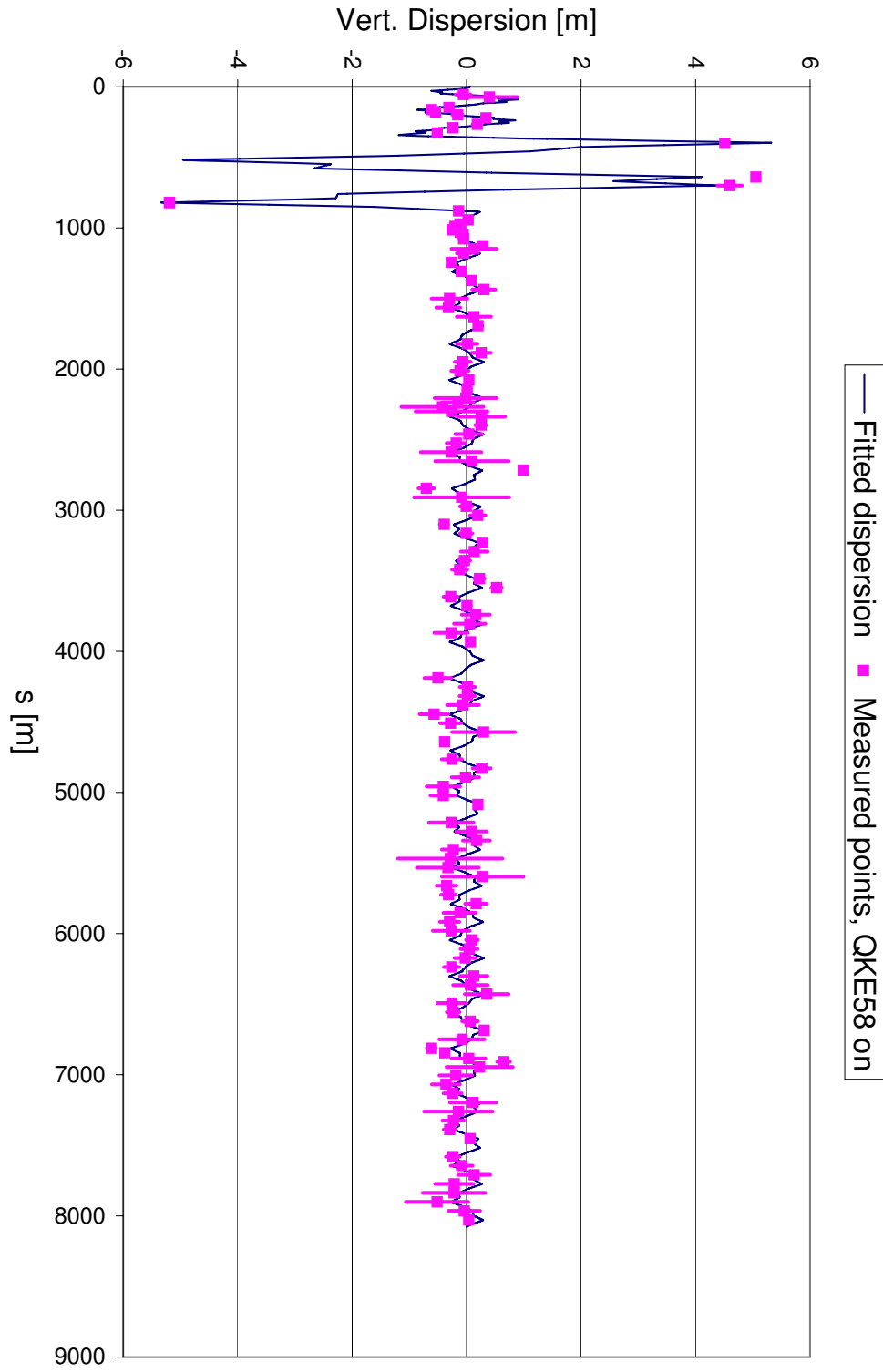
Figure 7: Vertical dispersion in TT2-TT10 and in the SPS 1st turn. QKE58 was on.
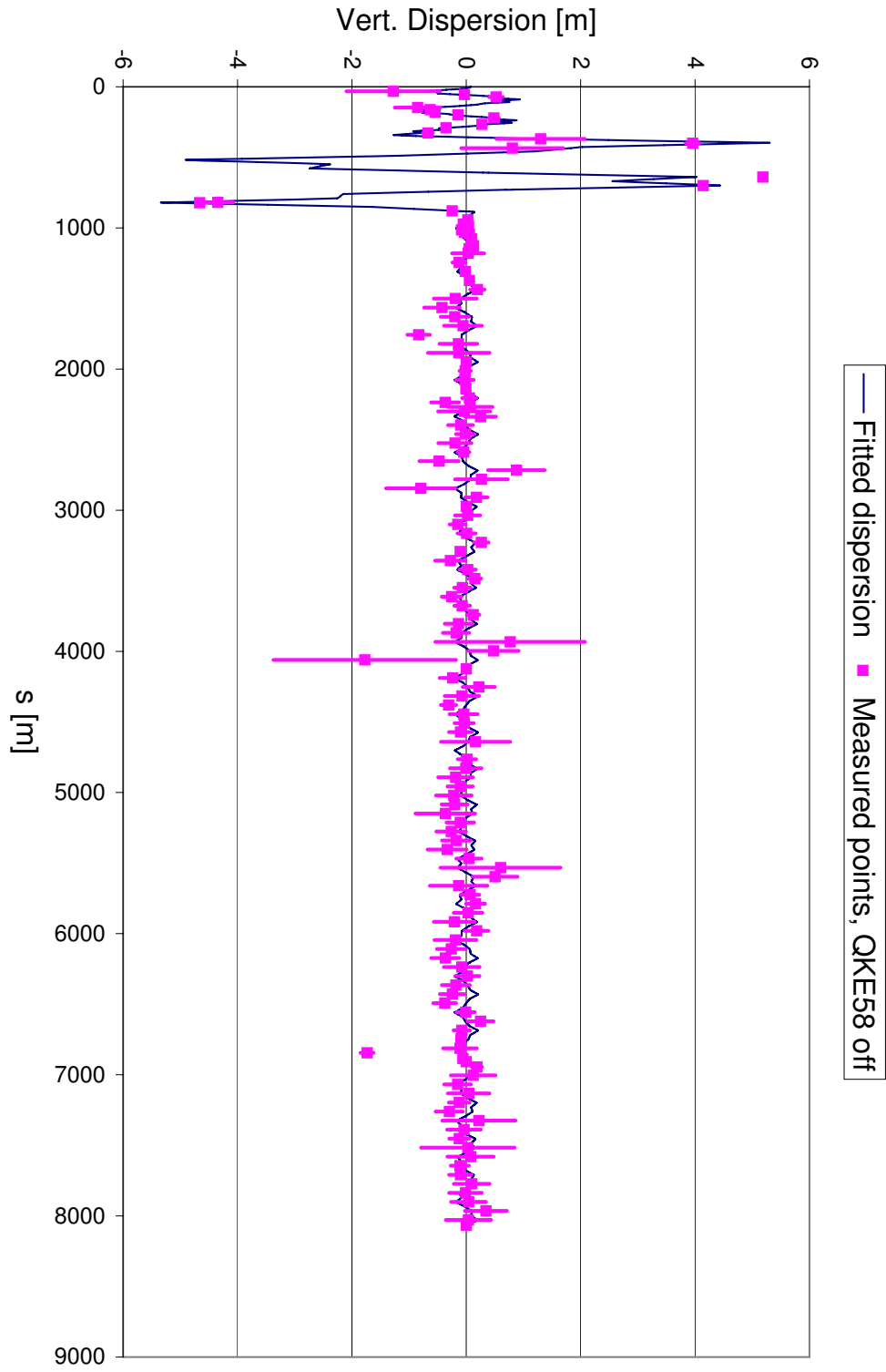
Figure 8: Vertical dispersion in TT2-TT10 and in the SPS 1st turn. QKE58 was off.

Monitor	$\sigma_i[mm]$	$\delta\sigma_i[mm]$	$D_i[m]$	$D_i^2(dp/p)^2/\sigma_i^2$	$screen_i$	θ_i	$\Sigma'^{(11)}_{C,i}/\sigma_i^2$
MTV201	1.659	0.018	0.756	1.6%	Ti-12	9.31E-06	0.0%
MSG257	0.786	0.010	2.038	52.6%	-	-	5.8%
MSG267	0.861	0.010	0.604	3.9%	-	-	2.4%
MSG277	1.346	0.010	-1.334	7.7%	-	-	0.0%
BTV1018	1.437	0.016	-2.447	22.7%	M-25	4.57E-06	3.1%
BTV1024	1.767	0.098	2.148	11.6%	M-25	4.57E-06	3.4%
BTV1025	1.184	0.012	-0.562	1.8%	M-25	4.57E-06	9.4%
BTV1026	1.339	0.010	-2.19124	21.0%	M-25	4.57E-06	8.5%

Table 6: Horizontal beam size measured at the monitors (with the error in its determination) and the quadratic contribution to the beam size (in %) coming from the dispersive part and from the Coulomb scattering at the OTR screens, as defined in Eq. 52 (QKE58 on)

Monitor	$\sigma_i[mm]$	$\delta\sigma_i[mm]$	$D_i[m]$	$D_i^2(dp/p)^2/\sigma_i^2$	$screen_i$	θ_i	$\Sigma'^{(11)}_{C,i}/\sigma_i^2$
MTV201	0.911	0.007	-0.044	0.0%	Ti-12	9.31E-06	0.0%
MSG257	1.117	0.010	-0.745	3.5%	-	-	2.9%
MSG267	1.252	0.010	-0.582	1.7%	-	-	1.2%
MSG277	1.468	0.010	-0.087	0.0%	-	-	0.0%
BTV1018	2.170	0.020	-5.184	44.7%	M-25	4.57E-06	1.4%
BTV1024	1.480	0.100	-0.310	0.3%	M-25	4.57E-06	4.9%
BTV1025	1.690	0.018	-0.361	0.4%	M-25	4.57E-06	4.6%
BTV1026	1.800	0.024	-0.27446	0.2%	M-25	4.57E-06	4.7%

Table 7: Vertical beam size (with the error in its determination) and contribution from the dispersion and the scattering at the screens (QKE58 on)

Monitor	$\sigma_i[mm]$	$\delta\sigma_i[mm]$	$D_i[m]$	$D_i^2(dp/p)^2/\sigma_i^2$	$screen_i$	θ_i	$\Sigma'^{(11)}_{C,i}/\sigma_i^2$
MTV201	2.037	0.015	-2.155	8.8%	Ti-12	9.31E-06	0.0%
MSG257	0.750	0.002	2.315	74.8%	-	-	8.0%
MSG267	0.996	0.003	-0.905	6.5%	-	-	0.0%
MSG277	1.700	0.007	-3.369	30.8%	-	-	1.2%
BTV1018	1.850	0.023	-4.518	46.8%	M-25	4.57E-06	0.7%
BTV1024	2.330	0.064	5.183	38.8%	M-25	4.57E-06	0.3%
BTV1025	1.345	0.013	0.542	1.3%	M-25	4.57E-06	7.5%
BTV1026	1.430	0.020	-2.58874	25.7%	M-25	4.57E-06	10.8%

Table 8: Horizontal beam size (with the error in its determination) and contribution from the dispersion and the scattering at the screens (QKE58 off)

Monitor	$\sigma_i[mm]$	$\delta\sigma_i[mm]$	$D_i[m]$	$D_i^2(dp/p)^2/\sigma_i^2$	$screen_i$	θ_i	$\Sigma'^{(11)}_{C,i}/\sigma_i^2$
MTV201	0.990	0.008	-0.041	0.0%	Ti-12	9.31E-06	0.0%
MSG257	1.048	0.005	-0.660	3.1%	-	-	3.2%
MSG267	1.100	0.006	-0.517	1.7%	-	-	1.5%
MSG277	1.591	0.010	-0.080	0.0%	-	-	0.0%
BTV.1018	2.420	0.030	-5.073	34.5%	M-25	4.57E-06	1.1%
BTV.1024	1.300	0.040	-0.411	0.8%	M-25	4.57E-06	6.3%
BTV.1025	1.540	0.011	-0.448	0.7%	M-25	4.57E-06	5.5%
BTV.1026	1.946	0.020	-0.28337	0.2%	M-25	4.57E-06	4.0%

Table 9: Vertical beam size (with the error in its determination) and contribution from the dispersion and the scattering at the screens (QKE58 off)
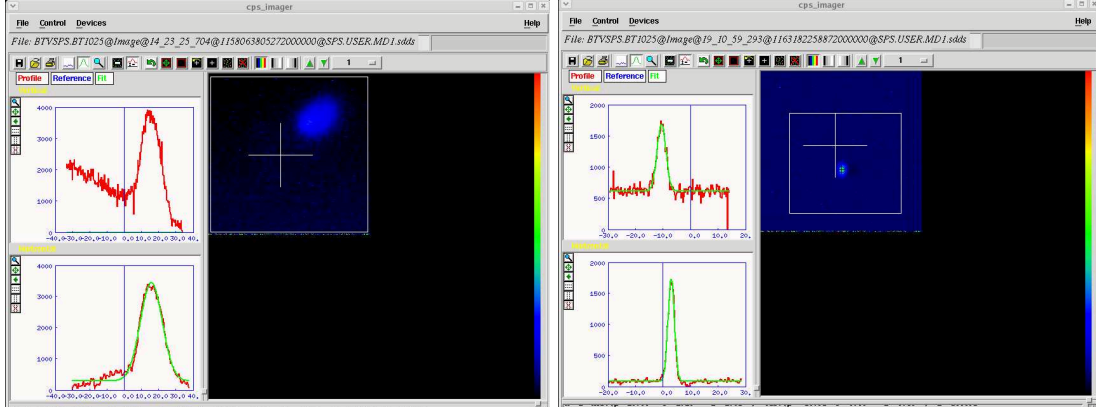
Figure 9: BTV1025 images before (left) and after (right) the replacement of the CCD camera intensifier. The beam characteristics and the size are similar.

	QKE58 ON		QKE58 OFF	
HORIZONTAL	with scattering	w/o scattering	with scattering	w/o scattering
D_0 [m]	2.9		3.9	
D'_0 [m]	0.348		0.380	
β[m]	24.854	25.575	25.103	25.488
α	-2.310	-2.458	-2.224	-2.336
ε[mm mrad]	1.177	1.279	1.402	1.516
H		1.004	1.006	1.0065

Table 10: Horizontal Twiss parameters at the beginning of TT2, LHC beam, with QKE58 on and off.

	QKE58 ON		QKE58 OFF	
VERTICAL	with scattering	w/o scattering	with scattering	w/o scattering
D_0 [m]	0.009		0.002	
D'_0 [m]	-0.0057		0.0005	
β[m]	10.447	10.432	11.130	11.064
α	1.168	1.175	0.883	0.896
ε [mm mrad]	1.133	1.170	1.202	1.245
H		1.000	1.063	1.056

Table 11: Vertical Twiss parameters at the beginning of TT2, LHC beam, with QKE58 on and off.

The Coulomb scattering at the OTRs is taken into account in the computation of the Twiss parameters, since the measurements have been done with all the screens inside the beam at the same time. The blow-up induced by the scattering at the screens which are before the monitor considered is not negligible and in the case of BTV1025 and BTV1026, it increases the horizontal σ_i^2 by up to a factor 10%.

The computation of the Twiss parameters has been done by solving the system of Eq. 23, replacing the $\sigma_{\beta,i}^2$ in Eq. 20 by the Eqs. 52 and 47, which take into account the scattering at the screens. In Tables 10 and 11 the horizontal and vertical Twiss parameters are summarized, for the cases with QKE58 on and off. The parameter H in the Tables, which corresponds to the mismatch factor (blow-up after filamentation) in [10], is defined as:

$$H = \frac{1}{2}\left[\frac{\beta_{on}}{\beta_{off}} + \left(\alpha_{on} - \alpha_{off}\frac{\beta_{on}}{\beta_{off}}\right)^2 \frac{\beta_{off}}{\beta_{on}} + \frac{\beta_{off}}{\beta_{on}}\right] \quad (67)$$
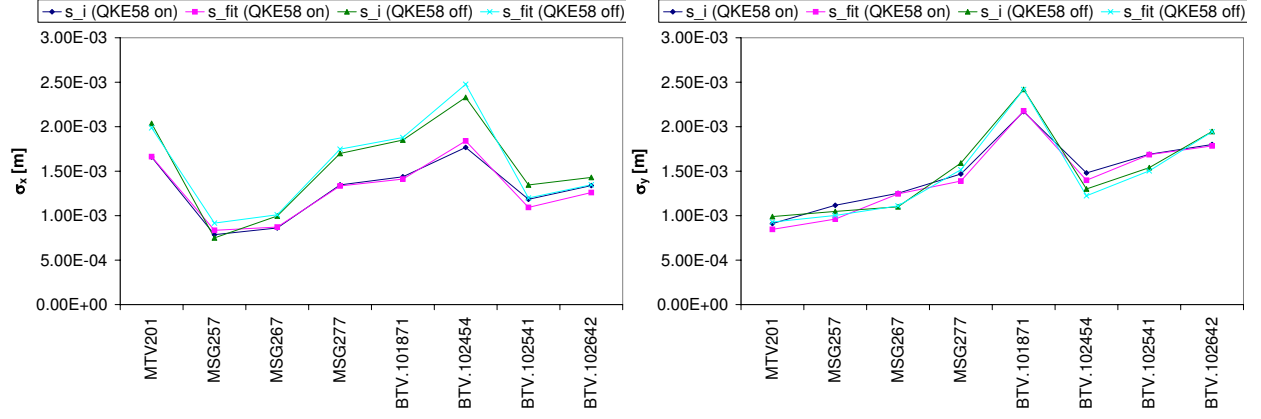
Figure 10: Horizontal (left) and vertical (right) beam size, for the cases with QKE58 on and off. Both the measured and the results from the fit are plotted

and in our case it is a measure of the variation of the phase-space ellipse computed at the beginning of TT2 with respect to the reference case (i.e. QKE58 on).

For the two cases there is almost no change in the Twiss parameters, although, in the measurements with QKE58 off, the computed emittance is 20% larger. In Fig. 10 are plotted the horizontal and vertical beam sizes at the monitors, for the cases with QKE58 on and off. The beam size is changing mainly because of the dispersion.

Figures 11 and 12 show the variation in the β– and α–functions, emittance and mismatch factor at the beginning of the line, when the initial dispersion or its derivative are different from the computed value. Since there are some uncertainty in the dispersion measurements, it is necessary to evaluate their effect on the Twiss parameters measurements. Assuming a 6% error on the measured horizontal dispersion (or on its derivative) at the beginning of the line, there is up to a 15% error on the computed β, α or ε, while the errors on the mismatch factor H is only a few percent.

5.2.1 Comparison with the model

There are some discrepancies between the results and the model [11], which is predicting a change in the phase-space beam-ellipse by a factor $H = 1.12$ in the horizontal plane by switching the QKE58 off, for the fast-extracted beams. To get these value, the beam parameters at the entry of the extraction septum `SMH16` are obtained by MAD-X computations with QKE58 on and off. A transfer matrix to the condition at the beginning of TT2 (at `QFO105`) is constructed from the measurements done with QKE58 on. The matrix so found is then used to predict the conditions at the beginning of the line with the QKE58 off.

The model predictions are summarized in Table 12. The increase in the dispersion is in agreement with the measurements, while the predicted large change in the Twiss parameters and in the mismatch factor are not found. Concerning the vertical plane, where the dispersion is small, the model predicts no appreciable mismatch, which is also found in the measurements.

MODEL	Horizontal	Vertical
D_0 [m]	4.67	0.009
D_0'	0.43	-0.006
β[m]	41.03	9.75
α	-4.050	0.876
H	1.12	1.04

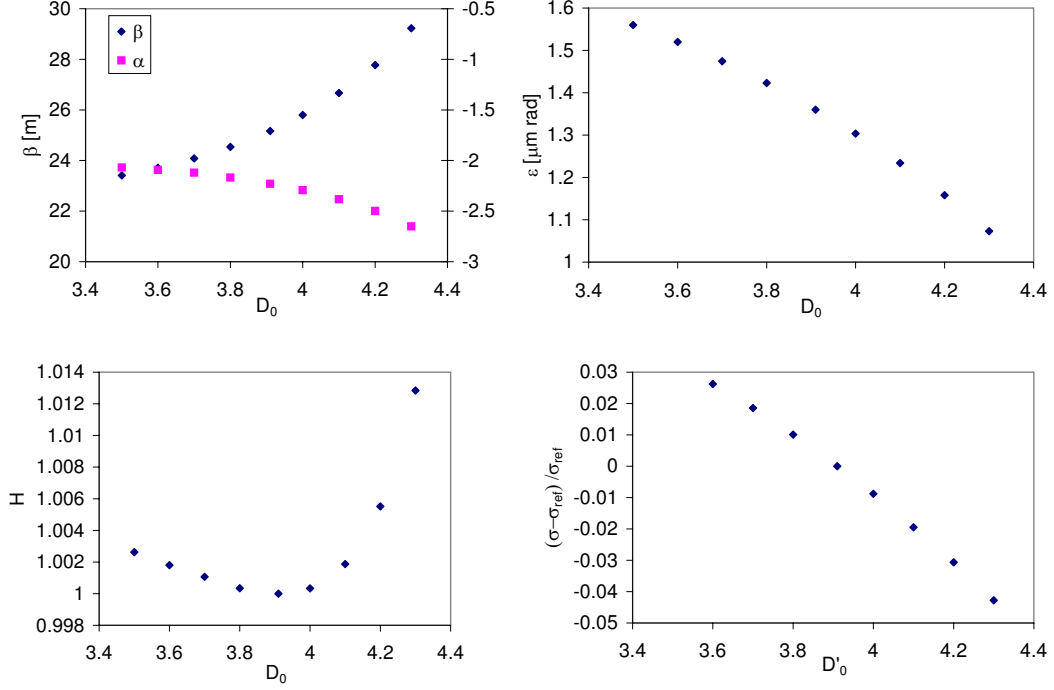Table 12: Twiss parameters model predictions for QKE58 off

24

Figure 11: α– and β–function, emittance, mismatch factor and beam size $\sigma = \beta\varepsilon$, at the beginning of the line, as a function of the initial dispersion, varying in an interval of $\pm 10\%$ around its computed value $D_0 = 3.91m$.
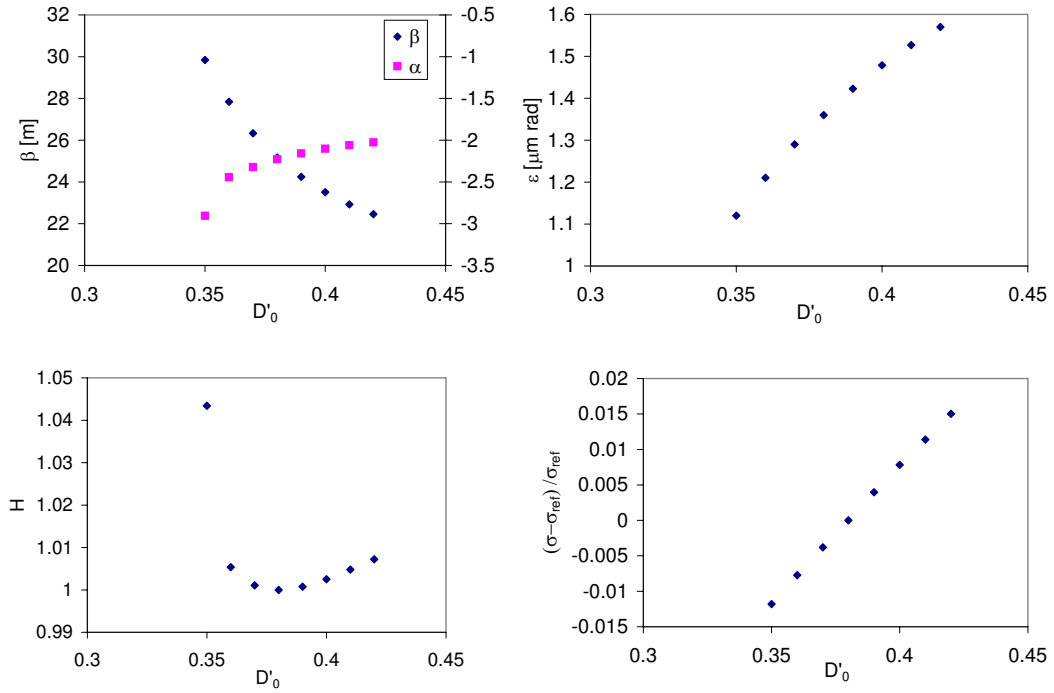

Figure 12: α– and β–function, emittance, mismatch factor and beam size $\sigma = \beta\varepsilon$, at the beginning of the line, as a function of the initial dispersion derivative, varying in an interval of $\pm 10\%$ around its computed value $D'_0 = 0.38$.

5.3 Measurements with AD beam

The effect of the QKE58 suppression has been also investigated for the AD beam, whose nominal parameters are listed in Table 13.

beam	AD
Energy	26GeV
Intensity	$1500\ 10^{10}p$
# bunches	4
ε_l	$2.83eVs$
ε_x^*	$10\mu m\ rad$
ε_y^*	$5\mu m\ rad$
dp/p	$5\ 10^{-4}$

Table 13: Nominal parameters of the AD beam used for the measurements of 11th November'06

Beam profiles have been taken with the SEM grids in TT2 (`MSG258`, `MSG268`, `MSG278`). These monitors where used as well to record the beam transverse position as a function of the beam momentum, varied from the PS, in order to extract the values of the dispersion at the grids. Tables 14 and 15 show the beam sizes and the computed dispersion at the monitors. The contribution, in %, from the dispersive part to the total beam size is also reported.

In Tables 16 and 17 the measured Twiss parameters at the beginning of TT2 and the computed mismatch factor (Eq.5.2) between the two configurations are listed. We were expecting a similar result to the MESPS beam, since the optics for the two beams and the extraction conditions should be similar. For the AD beam, instead, the measurements in the horizontal plane show no large increase in the dispersion but a considerable change in the Twiss parameters, leading to $H = 1.59$. The results for the Twiss parameters and emittance calculation go in the direction of what the model (Sec. 5.2.1 predicts for a fast-extracted proton beam at 26 GeV, but the small dispersion found in the case without QKE58 is unexpected. The measurements have been done with a nominal AD beam, whose horizontal emittance is 10 times larger then the MESPS beam. By varying the beam momentum energy for the dispersion measurements it is possible that some scraping has occurred at the extraction septum, thus altering the measurements. New measurements are planned in 2007, with a low intensity and low emittance beam.

HORIZ.	QKE58 ON				QKE58 OFF			
	σ_i [mm]	$\delta\sigma_i$ [mm]	$\mathbf{D}_i$ [m]	σ_D^2/σ_i^2	σ_i [mm]	$\delta\sigma_i$ [mm]	$\mathbf{D}_i$ [m]	σ_D^2/σ_i^2
MSG258	1.891	0.016	1.112	8.6%	1.791	0.041	1.032	8.3%
MSG268	3.117	0.038	1.125	3.3%	2.772	0.039	-0.401	0.5%
MSG278	3.180	0.075	0.211	0.1%	4.411	0.097	-1.504	2.9%

Table 14: Measured horizontal beam size (with the error in its determination) and dispersion at the SEMgrids, for the AD beam, with QKE58 on and off.

VERT.	QKE58 ON				QKE58 OFF			
	σ_i [mm]	$\delta\sigma_i$ [mm]	$\mathbf{D}_i$ [m]	σ_D^2/σ_i^2	σ_i [mm]	$\delta\sigma_i$ [mm]	$\mathbf{D}_i$ [m]	σ_D^2/σ_i^2
MSG258	2.066	0.020	0.424	0.3%	1.945	0.021	0.472	0.5%
MSG268	2.861	0.015	0.369	0.1%	2.796	0.036	0.401	0.2%
MSG278	3.235	0.032	0.103	0.0%	3.752	0.046	0.099	0.0%

Table 15: Measured vertical beam size (with the error in its determination) and dispersion at the SEM-grids, for the AD beam, with QKE58 on and off.

HORIZONTAl	QKE58 ON	QKE58 OFF
D_0 [m]	2.20	2.31
D_0'	0.236	0.181
β [m]	28.67	39.64
α	-3.118	-3.088
$\varepsilon*$ [μm rad]	11.92	10.15
H		1.59

Table 16: Horizontal Twiss parameters and mismatch factor at the beginning of TT2, for the AD beam.

VERTICAL	QKE58 ON	QKE58 OFF
D_0 [m]	-0.097	-0.096
D_0'	0.088	0.092
β [m]	8.47	10.35
α	0.937	0.826
$\varepsilon*$ [μm rad]	5.24	5.72
H		1.06

Table 17: Vertical Twiss parameters and mismatch factor at the beginning of TT2, for the AD beam.

6   Conclusions and plans for 2007

Measurements in TT2-TT10 line were performed in November 2006 with the MESPS beam (LHC proton beam at 26 GeV, with "low" longitudinal emittance) to investigate the effects of the QKE58 suppression in terms of changes in the Twiss parameters.

The dispersion measurements, in accordance with model prediction, show a variation of the horizontal dispersion at the beginning of the line from $2.9m$ to $3.9m$, when the QKE58 is switched off, and an increase of its maximum value in the line.

The existing Excel application has been improved, to treat separately different kind of monitors and to assign them a different calibration coefficient β_k. A difference of up to 90% has been found between the β_k in TT2 couplers and in the SPS BPM. In 2007 is planned a calibration campaign of the pick-ups in the line and in SPS, with MESPS beam, to verify these results.

Concerning the beam profiles measurements, the setting-up problems due to the BTVs electronics will be hopefully solved in the next measurements in 2007, since they will now be part of the new control system standard.

Contrary to the model, which predicts an 80% increase of the β_x when the QKE58 is off, leading to a mismatch factor between the two configurations of $H = 1.18$, the measurements show almost no change in the phase-space beam ellipse, when QKE58 is removed.

Especially in the horizontal plane, where the dispersion at the beam-profile monitors is large, the Twiss parameters and emittance values depend on the accuracy in determining the beam momentum spread, the dispersion and its derivative at the beginning of the line, therefore it is necessary to minimize the uncertainties on these values. Nevertheless, even if the Twiss parameters and emittance values are very sensitive to the dispersion, the beam ellipse it is not and the factor H show almost no change for a variation of the initial dispersion conditions.

New tools have been developed to analyze the 2D beam profiles at the OTR monitors. A new fitting routine is implemented to compute the Twiss parameters and emittance at the beginning of the line, by using the informations from all available monitors (SEM grids and BTVs). The Coulomb scattering at the OTR monitors is included in the computations, since, for the MESPS beam measurements performed with all the 5 screens inside the beam, it accounts for a factor 8% difference in the emittance determination.

Measurements with AD beam were also performed, showing a very small variation in the horizontal dispersion and a change in the beam phase-space ellipse by a factor $H = 1.59$ in the horizontal plane.

In 2007 a new measurement campaign is foreseen with both an LHC-type and the AD beam. In additions, it is required a calibration of the pick-ups of the line and the SPS, and, in order to better constrain the fit for the Twiss parameters, wire-scanners emittance measurements will also be taken in the PS and SPS.

The re-matching of the TT2-TT10 line for the new extraction conditions without QKE58 will then be finalized, by taking as a starting point the results of our measurements.

7 Acknowledgments

References

[1] R. Steeremberg, APC presentation, 6/10/06, (2006)

[2] G. Arduini, D. Jaquet, Dispersion measurement, AB-Note-2005-002 OP, (2005)

[3] H. Wiedemann, Particle Accelerator Physics, Springer ed., (1999)

[4] G. Arduini, M. Giovannozzi, K. Hanke, D. Manglunki, M. Martini, New Methods to Derive Optical and Beam Parameters in Transport Channels, Nucl. Instr. and Meth. A 459, 16-28, (2001)

[5] S. Turner (ed.), CAS 5th General Accelerator Physics Course, CERN 94-01, (1994)

[6] A.S. Muller, Description of Beam Matter interaction in the covariance matrix formalism, CERN/PS 2001-0013 AE, (2001)

[7] M. Della Negra, Multiple Coulomb Scattering of Beam Particles in the Phase Space Ellipse Formalism, SLAC-TN-71-1, (1971)

[8] GEANT, Detector Description and Simulation Tool, CERN Program Library Long Write-up W5013, March 1994, http://wwwasd.web.cern.ch/wwwasd/cernlib/version.html (1994)

[9] F. Roncarolo, Accuracy of the Transverse Emittance Measurements of the CERN Large Hadron Collider, PhD Thesis, Ecole polytechnique federale de Lausanne, (2005).

[10] G. Arduini, P. Raimondi, Transverse emittance blow-up due to injection errors, SL-Note-99-022 SLI, (1999)

[11] A. Franchi, private communication, in [12] (2007)

[12] E. Benedetto, APC presentation, 30/03/07, (2007)